ELSEVIER

International Journal of Solids and Structures 41 (2004) 1157–1172

INTERNATIONAL JOURNAL OF SOLIDS and STRUCTURES

www.elsevier.com/locate/ijsolstr

The mechanical behavior of a wire rope with an independent wire rope core

D. Elata *, R. Eshkenazy, M.P. Weiss

Faculty of Mechanical Engineering, Technion—Israel Institute of Technology, Technion City, Haifa 32000, Israel

Received 4 November 2003; received in revised form 4 November 2003

Abstract

A new model for simulating the mechanical response of a wire rope with an independent wire rope core is presented. The rope is subjected to both an axial load and an axial torque. In contrast with previous models that consider the effective response of wound strands, the present model fully considers the double-helix configuration of individual wires within the wound strand. This enables to directly relate the wire level stress to the overall load applied at the rope level. The model assumes a fiber response of individual wires. Two alternative kinematics of the wires are considered, and are used to predict the elastic response of the rope. The postulated kinematics are theoretically validated and the predicted rope response is in agreement with new experimental data. The new model enables the extraction of the stress at the wire level that can be used in turn to estimate global features of the rope such as force interaction between wires, rope stiffness, strength, and fatigue life.
© 2003 Elsevier Ltd. All rights reserved.

Keywords: Wire rope; Double-helix; Multi strand construction

1. Introduction

Most wire ropes are constructed from either a single strand, or from several strands that are wound around a core. This core may either be a strand in itself or it may be a fibrous or deformable element. The strand is constructed of wires that are wound around a central wire. In single, straight strands, all wound wires are each configured as a *single-helix*. However, in a wound strand each wire (except for the central wire of the strand) is configured as a *double-helix*.

The design of wire rope cross-sections dates back to the late 1800's (Sayenga, 1980), and has been continuously improved since. Many analytical studies of a multi-layer single strand construction have been proposed in literature (Cardou and Jolicoeur, 1997). Hruska (1952a,b) and Lanteigne (1985), modeled the mechanical response of a multi-layer single strand construction, assuming a fiber response of each wire (i.e., ignoring bending and torsion rigidity of the wires). Costello and Phillips (1976), Costello and Miller (1979),

* Corresponding author. Tel.: +972-482-931-84; fax: +972-483-245-33/482-957-11.
E-mail address: elata@tx.technion.ac.il (D. Elata).

0020-7683/$ - see front matter © 2003 Elsevier Ltd. All rights reserved.
doi:10.1016/j.ijsolstr.2003.11.021

Knapp (1979), McConnell and Zemke (1982) and Machida and Durelli (1973), extended the previous work by modeling the wires as rods, thus including the bending and torsion rigidity of the wires.

All the above studies were limited to a single, straight strand, in which all wound wires are single-helices. Jolicoeur and Cardou (1991) compared the mechanical response of a single strand rope as predicted by all the models mentioned above, and compared these models to experimental measurements of single strands. They showed that the simplifying assumption of fiber-like wires yields good results except for an inaccurate prediction of the torsion stiffness of the single straight strand.

However, most cables in use have a more complex cross-section in which most wires are configured as double helices. In order to model the complex cross-section of multi-strand constructions, several modeling approaches (Costello, 1990) have been suggested.

Velinsky (1981) and Velinsky et al. (1984) were the first to analyze the mechanical response of a multi-strand construction. They extended the procedure developed by Costello and Phillips (1976) and Costello and Miller (1979) to treat a multi-strand construction of frictionless wires. Their modeling procedure is based on the nonlinear equations of equilibrium of a thin helical rod (Love, 1944) and considers the torsion and bending stiffness of the wires.

Velinsky et al. computed the resultant tension and torque in a straight strand for uniform elongation and torsion of the straight strand. They then approximated the tension and torque of a wound strand that develop due to extension and twist of the wound strand by the same mechanical relation computed for the straight strand. To complete the model, they included the effect of changes in curvature of the wound strand by an approximation that considered planar bending of a straight strand around a cylinder.

Phillips and Costello (1985) generalized Velinsky's approach for any kind of wire rope with an Independent Wire Rope Core (*IWRC*). Their work considered the response of a rope bent over a sheave, and neglected friction forces between adjacent wires. This model was said to be applicable only to well-lubricated ropes or to ropes that are loaded exclusively in tension, without twisting or bending.

The models of Velinski and of Philips and Costello give a good approximation of the mechanical response of the rope. However, to obtain complete description of the stress in individual wires there is need to develop a model that will explicitly take into account the double helix construction (e.g., the geometrical treatment of Wang and McKewan (2001)). This complete description will enable to estimate resultant tension, bending and torsion moments, relative displacements and contact forces, and the variations of all these along the individual double-helix wires. This information is essential for predicting fatigue life, wear, and overall mechanical response of the entire rope.

It is difficult to conduct an analytical investigation of the mechanical response of wire rope because the kinematics of each wire is very complex. To facilitate an analytic study, it is therefore constructive to assume the kinematics of the wires, calculate the associated mechanical response of the whole construction, and examine the consequences of the assumptions by considering their affect on the validity of the equilibrium equations (Love, 1944).

In the present study, multi-strand constructions are analyzed while considering the double-helix geometry of the wires. In this study, the wires are treated as *fibers* that have no bending and torsion rigidity. This may seem to be a step backwards from previous studies that treated wires as rods. This simplification however enables rigorous and accurate consideration of the *double-helix* structure of individual wires in the rope.

The predicted mechanical response of multi-strand wire ropes are compared to experimental measurements using a tension–torsion machine designed and constructed in accordance with Feyrer (1994).

In the next section, the rope structure is described. Two possible kinematics of the wires are introduced in Section 3, where the mechanical response associated with each is formulated. The validity of each of the kinematics is discussed in Section 4, and case studies of specific rope cross-sections are examined in Section 5.

2. Rope structure

The rope is a straight structure constructed from layers of strands that are wound around the rope core (Fig. 1). It is convenient to describe the structure of the rope using a Cartesian coordinate system (X, Y, Z), with the Cartesian frame $\{\boldsymbol{e}_X, \boldsymbol{e}_Y, \boldsymbol{e}_Z\}$ where $\boldsymbol{e}_Z$ is the rope axis. The location along the centerline of a single-helix is given by

$$X_s = R_s \cos(\Theta_s) \tag{1a}$$

$$Y_s = R_s \sin(\Theta_s) \tag{1b}$$

$$Z_s = R_s \tan(\alpha_s)\Theta_s \tag{1c}$$

where R_s is the laying radius of the single-helix, α_s is the single-helix laying angle, and $\Theta_s = \Theta_0 + \Theta$. Here Θ is a free variable measuring the angle around the rope axis $\boldsymbol{e}_Z$ relative to $\boldsymbol{e}_X$, and $\Theta_0 = \Theta_{(Z=0)}$ is the single-helix phase angle. The strand centerline is a single-helix that is described by Eq. (1).

Following Andorfer (1983) and Feyrer (1994), the location along the centerline of a double-helix wire is given by

$$X_w = X_s(\Theta_s) + R_w \cos(\Theta_w)\cos(\Theta_s) - R_w \sin(\Theta_w)\sin(\Theta_s)\sin(\alpha_s) \tag{2a}$$

$$Y_w = Y_s(\Theta_s) + R_w \cos(\Theta_w)\sin(\Theta_s) + R_w \sin(\Theta_w)\cos(\Theta_s)\sin(\alpha_s) \tag{2b}$$

$$Z_w = Z_s - R_w \sin(\Theta_w)\cos(\alpha_s) \tag{2c}$$

where $\Theta_w = m\Theta_s + \Theta_{w0}$ and R_w is the distance between the double-helix wire centerline and the single-helix strand centerline. Here m is a construction parameter and Θ_{w0} is the wire phase angle. The construction parameter m is a geometrical property common to all wires in a specific wire layer within a strand.

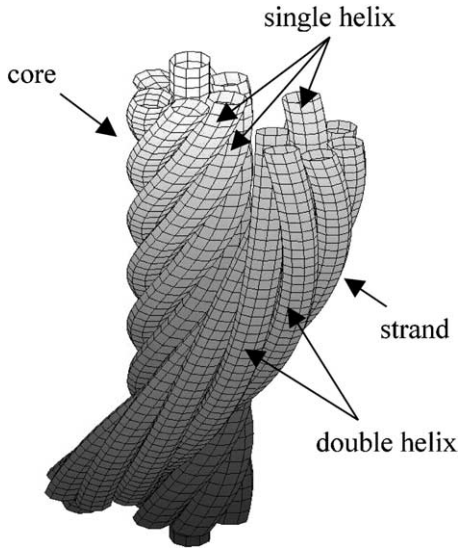

Fig. 1. The structure of a wire rope with an independent wire rope core (*IWRC*).

In the following analysis the *Frenet–Serret* frames $\{\boldsymbol{e}_T, \boldsymbol{e}_N, \boldsymbol{e}_B\}$ and $\{\boldsymbol{e}_t, \boldsymbol{e}_n, \boldsymbol{e}_b\}$ are used to describe the undeformed reference configuration and deformed configuration, respectively. Here $\boldsymbol{e}_T$ ($\boldsymbol{e}_t$) is the tangent unit vector, $\boldsymbol{e}_N$ ($\boldsymbol{e}_n$) is the principal normal and $\boldsymbol{e}_B$ ($\boldsymbol{e}_b$) is the binormal vector (Marsden and Tromba, 1988).

3. Kinematics of wires in a loaded rope

Consider a wire rope of a length L (Fig. 2) that is subjected to an axial displacement ΔL and an axial rotation angle $\Delta\varphi$. Exact analysis of the rope response to such edge displacements requires the simultaneous solution of the equilibrium equations of all wires considering inter-wire interaction. This is complicated due to the nonlinearity of the equilibrium equations and due to the complexity of the geometry. Therefore, approximate solutions that may facilitate the analysis are necessary. To this end, in this work, two alternative kinematic assumptions are examined. Each assumed kinematics uniquely defines the deformation of the centerline of each wire in the rope, and maps any point on a wire centerline to a new location. The extent to which the equilibrium equations are satisfied by the assumed kinematics is later used for validation.

The axial strain along a wire, due to an assumed kinematics is given by

$$\varepsilon = \frac{\mathrm{d}s}{\mathrm{d}S} - 1 \tag{3}$$

where $\mathrm{d}S$ is an incremental length along the undeformed wire, and $\mathrm{d}s$ is an incremental length along the deformed wire.

The two kinematics considered are associated with the two extreme cases of: (1) fully lubricated rope with no friction tractions between adjacent wires, and (2) unlimited friction between adjacent wires that disables relative displacements between them.

The description of the different kinematic assumptions may be simplified by considering imaginary sieves through which the rope wires are threaded. A rope-level sieve is perpendicular to the rope axis and

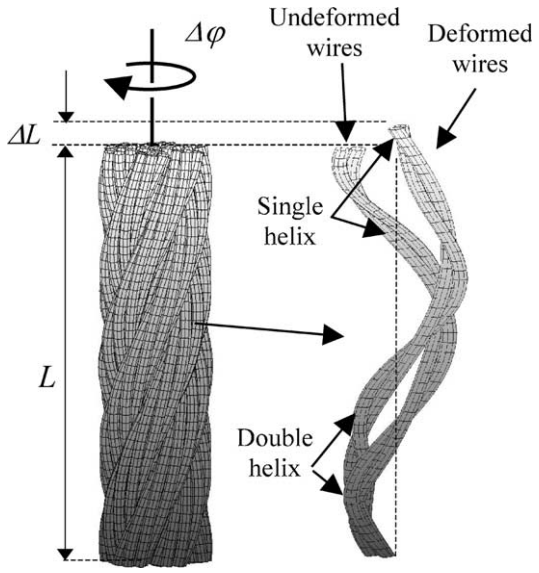

Fig. 2. A wire rope subjected to axial and rotational displacements.

preserves the relative position of the wire centerlines in the rope cross-section. The sieve itself may be axially displaced along the rope axis and may rotate relative to the rope axis. The sieve may be locked such that material points on the wires are fixed to the sieve, or it may be unlocked so that wires may freely slide through the sieve.

3.1. Locked rope-level sieves

The relative motion between neighboring sieves is uniform throughout the rope. Accordingly, the axial and rotational displacements of the rope-level sieve vary linearly along the rope axis. Under this assumption any rope cross-section perpendicular to the rope axis at the undeformed state remains planar and perpendicular to the rope axis in the deformed state. This kinematics induces a *variable* axial strain along each of the double-helix wires.

The location along the deformed centerline of a double-helix wire is given by:

$$x_w = \sqrt{X_w^2 + Y_w^2}\cos\left[\arctan\left(\frac{Y_w}{X_w}\right) + k_c Z_w\right] \tag{4a}$$

$$y_w = \sqrt{X_w^2 + Y_w^2}\sin\left[\arctan\left(\frac{Y_w}{X_w}\right) + k_c Z_w\right] \tag{4b}$$

$$z_w = Z_w(1 + \varepsilon_c) \tag{4c}$$

where k_c and ε_c are the cable twist and cable axial strain, respectively,

$$k_c = \frac{\Delta\phi}{L} \tag{5a}$$

$$\varepsilon_c = \frac{\Delta L}{L} \tag{5b}$$

Fig. 2 illustrates the undeformed and deformed configurations of a single-helix and a double-helix wire in a rope that is subjected to both twist and cable axial strain.

3.2. Unlocked rope-level sieves

In this kinematics, the wire centerlines are located along the same spatial curves as in the previous kinematics, Eq. (4). However, in this kinematics each individual wire is free to slide through the unlocked sieves along its related spatial curve. Due to the assumption of fiber response the axial strain is uniform along the centerline of each of the wires. In a rope of infinite length the uniform strain is identical for all wires from the same layer in a strand. In a rope of finite length, the wires are fixed at the rope ends and consequently the uniform strain in each wire in a given strand layer may vary.

In this kinematics, a cross section does not remain planar in the deformed configuration and relative (out of sieve-plane) displacements between adjacent wires develop.

At each of the above kinematics, radial contraction due to Poisson effect on the wire diameter is neglected on the basis of previous work (Jolicoeur and Cardou, 1991). Similarly, it is assumed that in the case of *IWRC* construction the radial contraction of the rope core may also be neglected. The behavior of a wire rope with fiber core in which radial contraction may not be neglected is not considered in the present study.

4. Validation of the kinematics

By substituting an assumed kinematics into the equilibrium equation of each wire, the external loads that are required to enable the kinematics are derived. It is assumed that these external loads are applied by adjacent wires. However, the resultant of the external loads applied to all wires at any given rope cross-section, is an external load that is applied to the rope. As the rope is loaded only at its ends, this rope-level external load must vanish. The amplitude of the associated rope-level external loads is a measure of the validity of the assumed kinematics.

4.1. Spurious loads

Consider an interval $[s_0\, s]$ along a wire (fiber in this case) illustrated in Fig. 3. In this figure, s is the length along the wire, T is the axial tension, and $\boldsymbol{q}$ is the traction (force per unit wire length) applied to the wire. The equilibrium equation of the wire in this interval is given by

$$-T(s_0)\boldsymbol{e}_t(s_0) + T(s)\boldsymbol{e}_t(s) + \int_{s_0}^{s} \boldsymbol{q}(s)\mathrm{d}s = 0 \tag{6}$$

Differentiation of this equation with respect to s yields

$$\boldsymbol{q} = -\frac{\mathrm{d}T}{\mathrm{d}s}\boldsymbol{e}_t - T\kappa\boldsymbol{e}_n \tag{7}$$

where κ is the local curvature, and $\kappa\boldsymbol{e}_n = \frac{\partial \boldsymbol{e}_t}{\partial s}$. Eq. (7) is a specific case of the more general equilibrium equations for a naturally curved rod derived by Kirchhof (Love, 1944).

At every cable cross-section the resultant $\boldsymbol{Q}(z)$ of all these tractions (force per unit rope length), and the resultant traction-moment $\boldsymbol{M}(z)$ of all these tractions with respect to the cable axis, are given by

$$\boldsymbol{Q}(z) = \sum_{i=1}^{n_w} \left[\boldsymbol{q}_i(z)\frac{\mathrm{d}s_i(z)}{\mathrm{d}z}\right] \tag{8a}$$

$$\boldsymbol{M}(z) = \sum_{i=1}^{n_w} \left[\boldsymbol{r}_i(z) \times \boldsymbol{q}_i(z)\frac{\mathrm{d}s_i(z)}{\mathrm{d}z}\right] \tag{8b}$$

where $\boldsymbol{q}_i$ and $\mathrm{d}s_i$ are the traction and length differential relate to wire i, $\boldsymbol{r}_i$ is the location of the centerline of wire i with respect to the cable axis and n_w is the number of wires. In a cable that is loaded at its edges, $\boldsymbol{Q}(z)$ and $\mathbf{M}(z)$ should vanish if no external loads are applied along the rope.

Let $\boldsymbol{F}_c$ be the resultant internal force at the cable-level cross-section, and let $\boldsymbol{M}_c$ be the resultant internal moment at the cable-level cross-section with respect to the cable axis

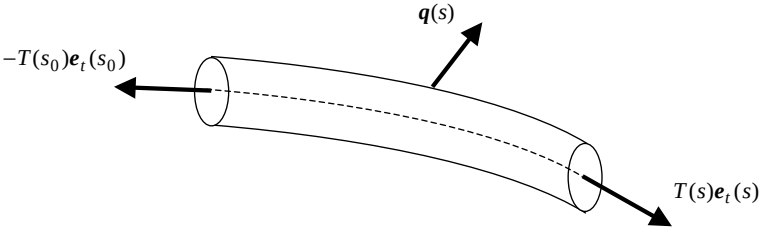

Fig. 3. A schematic view of a loaded wire segment.

$$\boldsymbol{F}_{\mathrm{c}}(z) = \sum_{i=1}^{n_{\mathrm{w}}} T_i(z)\boldsymbol{e}_{t_i}(z) \tag{9a}$$

$$\boldsymbol{M}_{\mathrm{c}}(z) = \sum_{i=1}^{n_{\mathrm{w}}} \boldsymbol{r}_i(z) \times T_i(z)\boldsymbol{e}_{t_i}(z) \tag{9b}$$

Due to equilibrium at the cable level, any nonzero value of $\boldsymbol{Q}(z)$ and $\boldsymbol{M}(z)$ will appear as variations in $\boldsymbol{F}_{\mathrm{c}}$ and $\mathbf{M}_{\mathrm{c}}$ along the cable, respectively. Accordingly, the variation of $\mathbf{F}_{\mathrm{c}}$ and of $\boldsymbol{M}_{\mathrm{c}}$ may be considered instead of directly computing $\boldsymbol{Q}(z)$ and $\boldsymbol{M}(z)$.

All cable cross-sections considered in this work have more than a two-fold rotational symmetry with respect to the cable axis, and therefore the resultant force and moment at the cable cross-section are axial ($\boldsymbol{F}_{\mathrm{c}} \times \boldsymbol{e}_z = 0$; $\boldsymbol{M}_{\mathrm{c}} \times \boldsymbol{e}_z = 0$). The magnitude of the axial force and the magnitude of the moment at the cable cross-section are therefore

$$F_{\mathrm{c}} = \boldsymbol{F}_{\mathrm{c}} \cdot \boldsymbol{e}_z \tag{10a}$$

$$M_{\mathrm{c}} = \boldsymbol{M}_{\mathrm{c}} \cdot \boldsymbol{e}_z \tag{10b}$$

Finally, the variations of F_{c} and M_{c} are given in a normalized form by

$$V_F(z) = \frac{F(z) - \overline{F}_{\mathrm{c}}}{\overline{F}_{\mathrm{c}}} \tag{11a}$$

$$V_M(z) = \frac{M(z) - \overline{M}_{\mathrm{c}}}{\overline{M}_{\mathrm{c}}} \tag{11b}$$

where $\overline{F}_{\mathrm{c}}$ and $\overline{M}_{\mathrm{c}}$ are the average values of $F_{\mathrm{c}}(z)$ and $M_{\mathrm{c}}(z)$ along the cable, respectively.

The validity of an assumed kinematics will be henceforth quantified by the maximal value of the variations of V_F and V_M.

4.2. Reciprocity theorem of Betti

A characteristic cable feature is the coupling of extension and torsion responses. In the linear case, the global cable stiffness and coupling effect can be conveniently expressed as (Jolicoeur and Cardou, 1991)

$$\begin{Bmatrix} F_{\mathrm{c}} \\ M_{\mathrm{c}} \end{Bmatrix} = \begin{bmatrix} a_{11} & a_{12} \\ a_{21} & a_{22} \end{bmatrix} \begin{Bmatrix} \varepsilon_{\mathrm{c}} \\ k_{\mathrm{c}} \end{Bmatrix} \tag{12}$$

The cable as a structure may be considered as an elastic body that is subjected to two uncoupled external loads. According to the reciprocity theorem of Betti, the stiffness matrix must be symmetric. Jolicoeur and Cardou (1991) showed that models of single strand ropes satisfy this condition. The validity of the postulated kinematics in this work, will be also quantified by the extent in which the Betti theorem is satisfied, namely, the symmetry of the stiffness matrix in Eq. (12). This validation is also a measure of the spurious external loads at the rope level because in the absence of such loads Betti's theorem is naturally satisfied.

5. Simulation and comparison to experimental data

To measure the mechanical response of rope specimens, a tension torsion machine was constructed (Fig. 4). In this testing machine, the cable is subjected to an axial elongation. The cable is fully clamped at the upper grip while the lower grip may be either free to rotate or is locked at a fixed rotation angle. The test

Fig. 4. The tension–torsion test machine. (a) An encoder measures the rotation angle, and a load cell measures the torque. (b) Two *LVDT* devices measure the extension of the cable.

machine is designed to withstand an axial load of up to 150 kN. The rope specimen is 1500 mm in length and is clamped by two sockets at its ends. A bearing (Fig. 4a) connected to the axial load cell enables a free end condition. A load cell located at the edge of a radial cantilever measures the axial torque developed when the rotational degree of freedom is locked.

Two LVDT devices (Fig. 4b) measure the extension of the cable with accuracy of ±0.02 mm. The measurement procedure follows Feyrer (1990) and involves ten loading cycles of up to ~70% of the ultimate breaking load (*UBL*), and then measuring the stiffness in cycles of unloading/reloading with small load variations. Under fixed ends condition the axial elongation is measured by the LVDT devices that are attached by grips to the ends of gauging rods that are parallel to the rope. These rods are attached to a ring grip, which is rigidly fixed to the other end of the rope near the sockets. Under free end condition the axial elongation is measured relative to the bottom bearing (to avoid the influence of the grip twisting on the

measurement). To this end it was verified that the frame is sufficiently rigid so that the frame deformations are totally negligible relative to the cable deformation under a free end condition.

The simulation programs were written in the Maple™ symbolic programming code. The simulation procedure included the following steps:

1. Characterization of the geometrical parameters of all wires in the undeformed configuration.
2. Determination of the deformed configuration of each wire according to the postulated kinematics.
3. Calculation of the axial strains of each wire at any cable cross-section.
4. Computation of the rope level internal axial force and internal axial torque, at any given cross-section.
5. Determination of the variations in the rope level axial force and torque.
6. Calculation of the stiffness matrix coefficients of the rope.

The mechanical response of two specific cables are measured and simulated:

(1) A 6×36 *IWRC* rotating rope of 14 mm diameter (Fig. 5). The cable is constructed of a strand core, an inner stand layer of right lang-lay, and an outer strand layer of a right regular-lay.
(2) A 18×7 *IWRC* non-rotating rope of 14 mm diameter (Fig. 6). The cable is constructed of a strand core, an inner stand layer of left lang-lay, and an outer strand layer of a right regular-lay.

First, to examine the implications of locked and unlocked sieves, the simulated axial strain of a wire in the external layer of an external strand of the 6×36 rotating rope, is plotted (Fig. 7). The axial strain under locked sieve kinematics periodically varies by 22% from its average value. The larger strain occurs where the radial location of the wire is maximal, as can be expected in a regular lay. In Fig. 8, simulations of the

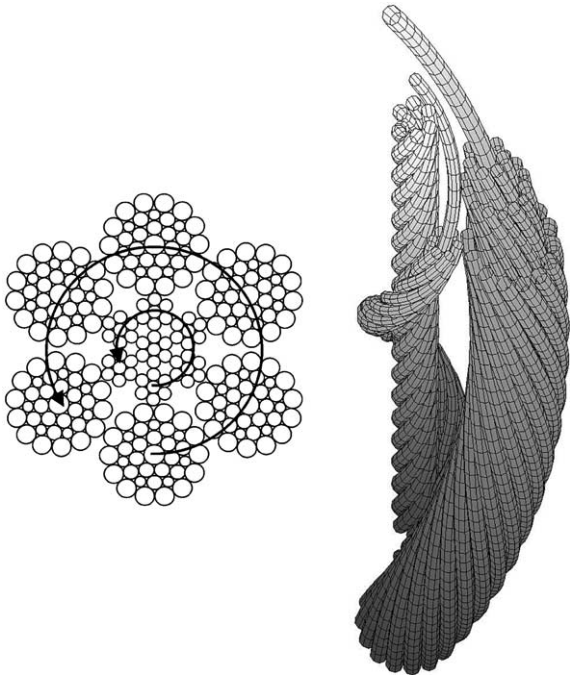

Fig. 5. Rotating 6×36 rope *IWRC*. A schematic description of the strands construction and a rope cross-section.

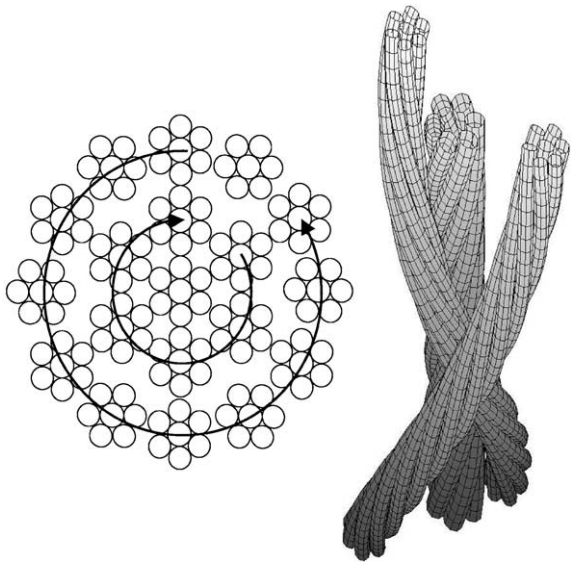

Fig. 6. Non-rotating 18×7 rope *IWRC*. A schematic description of the strands construction and a rope cross-section.

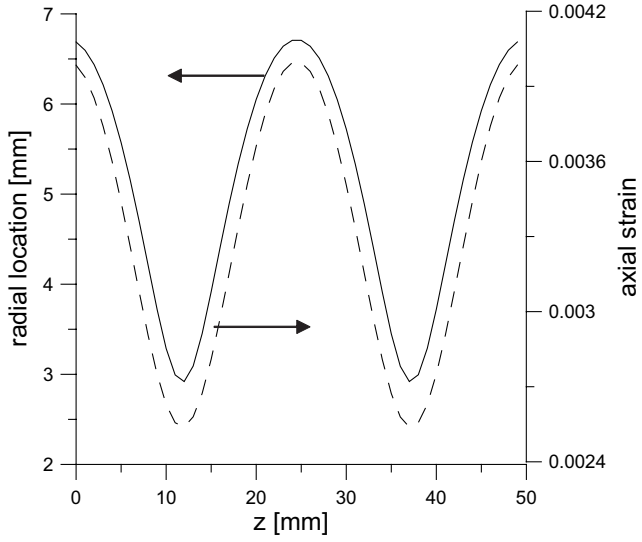

Fig. 7. Axial strain and radial location of a wire along the rope axis. The wire is from the external layer of the external strand of the 6×36, regular lay ($\varepsilon_c = 0.004$, $k_c = -0.001$).

same parameters are plotted for a lang-laid wire in a rope with an identical cross-section. As expected for a lang-laid wire, the larger strain occurs where the radial location is minimal (i.e., maximal axial stress at the wire level occurs deep within the rope).

For all simulations executed in this work the variations V_F in the axial force F_c and the variations V_M in the moment M_c at the cable cross-section were less than 1.0e−7. This suggests that both assumed kinematics are reasonable approximations of the actual deformation of the wires.

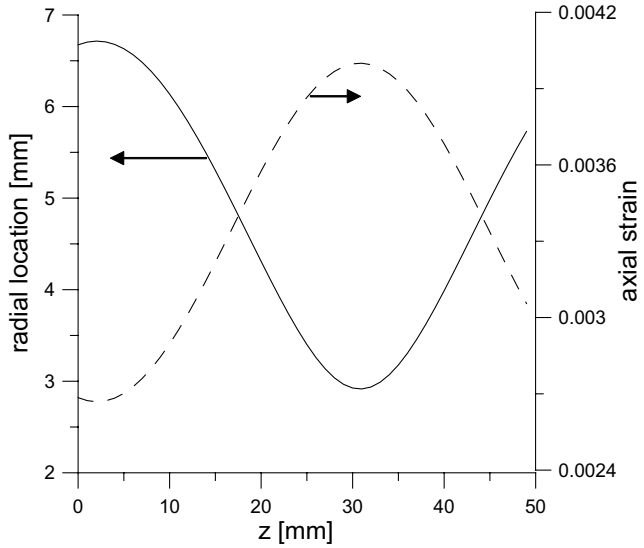

Fig. 8. Axial strain and radial location of a wire along the rope axis. The wire is from the external layer of the external strand of the 6×36, lang lay ($\varepsilon_c = 0.004$, $k_c = -0.001$).

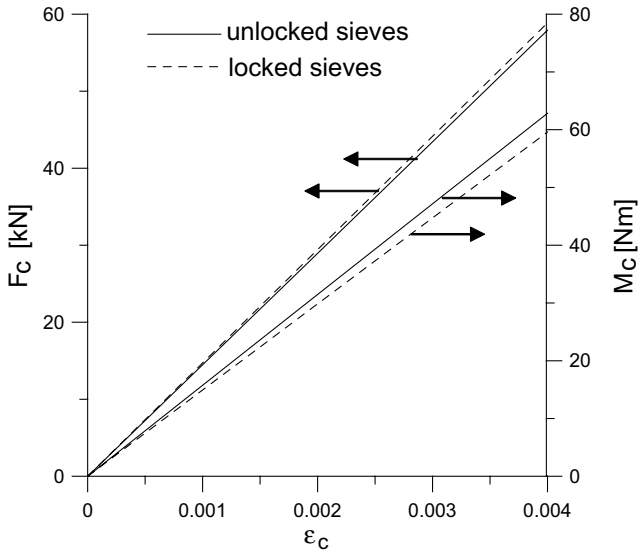

Fig. 9. Simulated axial force and axial torque for the 6×36 rotating rope, under fixed end condition.

Figs. 9–12 present the simulated axial force and torque for both ropes as function of the applied axial elongation and rotational strain, for the free and fixed end-conditions. For all the different cases the response is nearly linear.

Under fixed end condition the tension–elongation ratio (a_{11}) predicted by the locked sieves kinematics is slightly higher than that predicted by the unlocked sieves (~1.5% difference between the two kinematics).

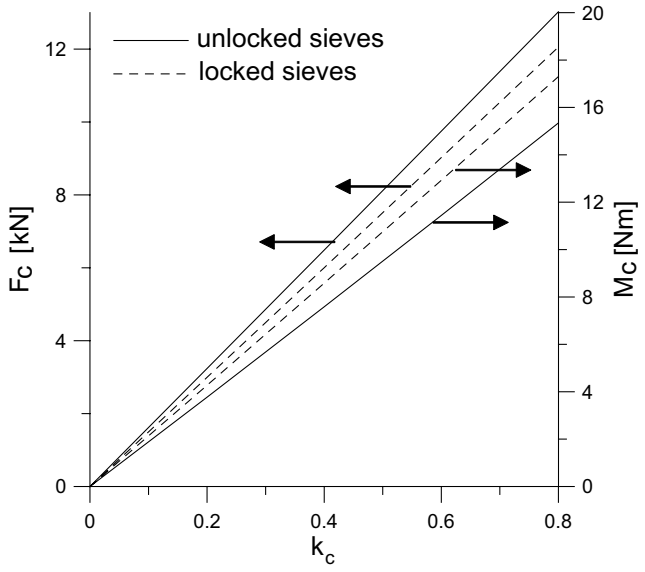

Fig. 10. Simulated axial force and axial torque for the 6×36 rotating rope, open end.

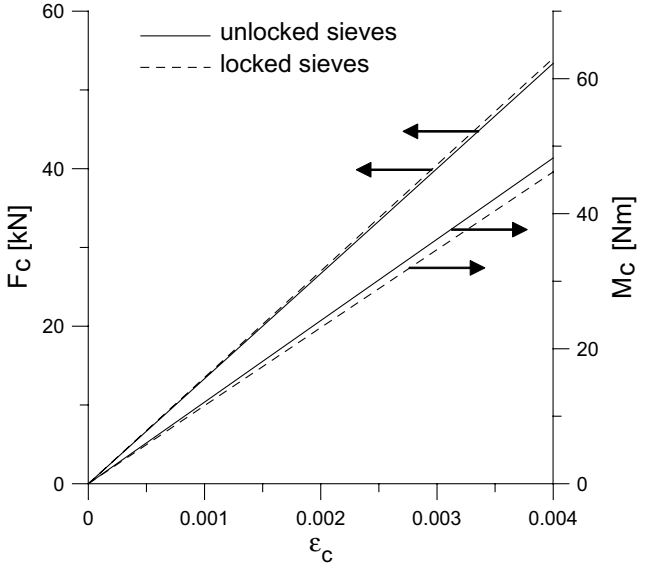

Fig. 11. Simulated axial force and axial torque for the 18×7 rotating rope, under fixed end condition.

In contrast, under fixed end conditions the torque–elongation ratio (a_{21}) predicted by the locked sieves kinematics is lower than that predicted by the unlocked sieves (~5% difference between the two kinematics).

Under free end condition the tension–rotation ratio (a_{12}) predicted by the locked sieves kinematics is lower than that predicted by the unlocked sieves (~3.5% difference between the two kinematics). For the

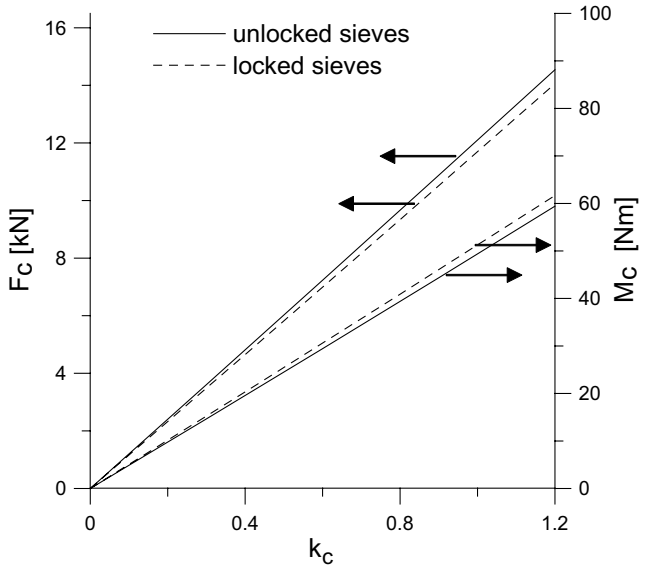

Fig. 12. Simulated axial force and axial torque for the 18×7 rotating rope, open end.

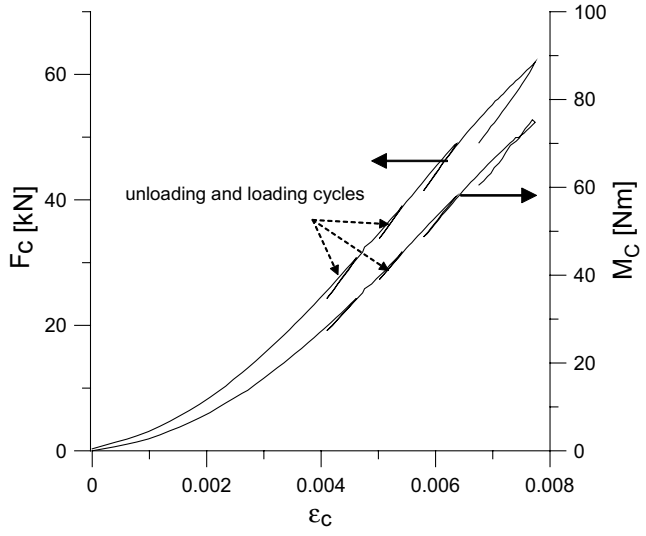

Fig. 13. Loading test of the 18×7 non-rotating rope under fixed ends condition.

same free end conditions the torque–rotation ratio (a_{22}) predicted by the locked sieves kinematics is higher than that predicted by the unlocked sieves (~15% difference between the two kinematics for the rotating cable, and ~5% for the non-rotating cable).

Fig. 13 describes the measured axial force and measured axial moment as function of axial strain, for the 6×36 rope under fixed-end conditions. The initial response is non-linear in contrast to the prediction in Fig. 9. The stiffness coefficients of the rope were calculated from three unloading–reloading cycles. Fig. 14

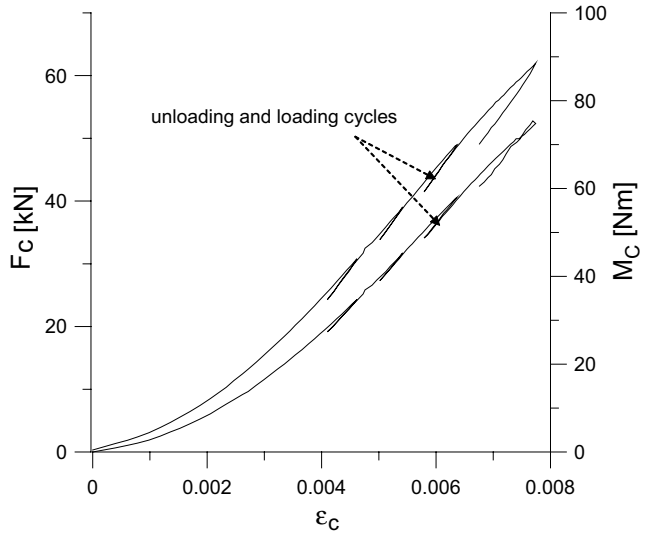

Fig. 14. Loading test of the 6×36 rotating-rope under fixed ends condition.

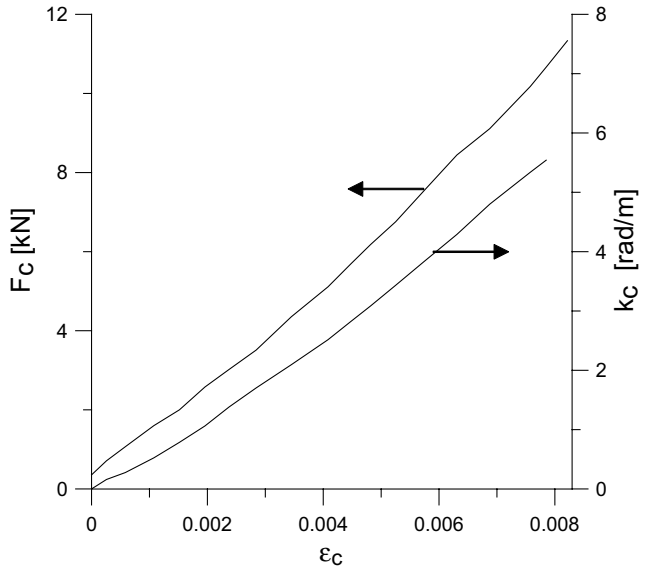

Fig. 15. Rotational strain versus axial strain as measured for the 6×36 rotating rope under a free end condition.

describes the measured axial force and measured axial moment as function of axial strain, for the 18×7 non-rotating rope under fixed end conditions. The initial response is more linear than that of the non-rotating rope (Fig. 13).

Fig. 15 presents the axial load and rotational stain as function of the applied axial strain for the 6×36 rope. The free end condition measurement was not conducted on the 18×7 rope because it is a non-rotating rope.

Table 1
Calculated and measured stiffness matrix coefficients

Cable		$a_{11}[N]\times10^7$	a_{12} [KNm/rad]	a_{21} [KNm]	a_{22} [Nm^2/rad]	a_{21}/a_{22}	$\frac{a_{21}-a_{12}}{a_{21}}$ [%]
18×7 non-rotating 14 mm	Measured	1.15	–	−9.762	–	–	
	Unlocked rope-level sieves	1.33	11.95	12.06	49.36	244	0.6
	Locked rope-level sieves	1.35	11.55	11.69	51.30	227	1.9
	Costello rod model	1.34	12.74	12.64	50.80	248	0.8
6×36 rotating 14 mm	Measured	1.30	16.15	15.50	19.2	700	
	Unlocked rope-level sieves	1.447	15.8	15.72	18.25	861	3.4
	Locked rope-level sieves	1.47	15.05	14.89	21.57	690	1.8
	Costello rod model	1.469	17.12	16.97	21.59	786	0.88

Table 1 summarizes all measured and calculated stiffness matrix coefficients. Also included is a comparison to Velinski's and Costello's model. The table presents the coefficients as simulated by their model. Poisson's effect was not considered. For both cables the torsion coefficients (a_{21}, a_{22}, a_{12}) as predicted by both kinematics are lower relative to the values as predicted by Costello and Velinski's model. Negligible differences exist between the axial coefficients (a_{11}, a_{12}). Under fixed end condition the tension–elongation ratio (a_{11}) predicted by locked sieves kinematics is slightly higher than that predicted by unlocked sieves kinematics.

The stiffness matrix is nearly symmetric for both kinematics (a deviation of 1–3%, see Table 1). Also, as previously mentioned, the variations in the axial force and moment at the rope level are less than 1.0e−7.

The simulated results are in agreement with the experimental data. For both cables the axial stiffness coefficient (a_{11}) simulated by locked and unlocked sieves is larger than the stiffness measured under fixed end condition. The lower measured values may be due to deformation at the contact point between wires, which are not considered here. Overall, the difference between simulated and measured stiffness coefficients is in the range of up to 20%, based on measurements of a single specimen for each rope.

6. Discussion and conclusions

A new model of the mechanical response of a wire rope with multi-strand construction is proposed. The model explicitly accounts for the double helix configuration of independent wires. The model is based on a postulated kinematics of individual wires within the rope. Specifically, two possible kinematics are considered: open sieves that emulate a well lubricated rope, and closed sieves that emulate infinite friction between adjacent wires. The two kinematics predict a slightly different rope response, but at the *wire* level, the axial stress predicted by the two kinematics is considerably different.

The model also includes a theoretical means of quantitatively validating the postulated kinematics for any rope structure (diameter and construction and laying angles). To further validate the new model, experimental data was collected. To this end, the mechanical response of two cables was measured using a tension–torsion machine. The rope level stiffness matrix coefficients predicted by the model are in overall agreement with the experimental data. The predicted coefficients are a little higher than the measured

values. This may be due to local effects such as enhanced deformation at inter-wire contacts that are not included in the model.

The proposed model provides wire level predictions of the tensile stress, axial strain, integrated inter-wire interactions and friction forces. This information can be used to predict failure, fatigue and fretting at the wire level. Accordingly, the model can be used for designing rope cross-sections with optimal properties such as rotation-resistant and a more uniform load distribution between the wires.

Jolicoeur and Cardou (1991) compared various strand models (single-helix configurations) and have found that the various predictions of the strand-level response were only slightly affected by inclusion of bending and torsion rigidities of individual wires. However, it seems that the bending and torsion rigidities may be important for better estimation of wire-level stress (Schiffner, 1986). Inclusion of the torsion and bending rigidities of individual wires into the presented double-helix model may be a subject for further study.

References

Andorfer, K., 1983. Die Zugkraftverteilung in schwingend beanspruchten geraden Seilen, Ph.D. Dissertation, TU Graz.

Cardou, A., Jolicoeur, C., 1997. Mechanical models of helical strands. App. Mech. Rev. 50 (1), 1–13.

Costello, G.A., 1990. Theory of Wire Rope. Springer-Verlag, New York.

Costello, G.A., Miller, R.E., 1979. Lay effect of wire rope. J. Eng. Mech. Div. ASCE 105, 597–608, No. EM4, Paper 14753.

Costello, G.A., Phillips, J.W., 1976. Effective modulus of twisted wire cables. J. Eng. Mech. Div., ASCE 102, 171–181.

Feyrer, K., 1990. Seilelastizitatsmodul von Rundlitzenseilen. DRAHT 41 (4), 498–504.

Feyrer, K., 1994. Drahtseile. Springer-Verlag, Berlin, Heidelberg.

Hruska, F.H., 1952a. Radial forces in wire ropes. Wire and Wire Products 27, 459–463.

Hruska, F.H., 1952b. Tangential forces in wire ropes. Wire and Wire Products 28, 459–463.

Jolicoeur, C., Cardou, A., 1991. A numerical comparison of current mathematical models of twisted wire cables under axisymmetric loads. J. Energy Res. Tech. 113, 241–249.

Knapp, R.H., 1979. Derivation of a new stiffness matrix for helically armoured cables considering tension and torsion. Int. J. Num. Meth. Eng. 14, 515–529.

Lanteigne, J., 1985. Theoretical estimation of the response of helically armored cables to tension, torsion, and bending. J. Appl. Mech 52, 423–432.

Love, A.E.H., 1944. A Treatise on the Mathematical Theory of Elasticity, Chaps. 18 and 19. Dover Publications, New York.

Machida, S., Durelli, A.J., 1973. Response of a strand to axial and torsional displacements. J. Mech. Eng. Sci. 15, 241–251.

Marsden, J.E., Tromba, A.J., 1988. Vector Calculus, third ed. Freeman and Co., New York.

McConnell, K.G., Zemke, W.P., 1982. A model to predict the coupled axial torsion properties of ASCR electrical conductors. Exp. Mech. 22, 237–244.

McKewan, R.C, McKewan, W.M., 2001. A model for the structure of round-strand wire ropes. O.I.P.E.E.C. Bull. 81, 15–42.

Phillips, J.W., Costello, G.A., 1985. Analysis of wire ropes with internal wire rope cores. Trans. ASME 52, 510–516.

Sayenga, D., 1980. The birth and evaluation of the american wire rope industry. In: First Annual Wire Rope Proceedings, Engineering Extension Service, Washington State University, Pullman, Washington.

Schiffner, G., 1986. Spannungen in laufenden Drahtseilen, Ph.D. dissertation, Universitaet Stuttgart.

Velinsky, S.A., 1981. Analysis of wire ropes with complex cross sections, Ph.D. thesis, Department of Theoretical and Applied Mechanics, University of Illinois at Urbana-Champaign, 87.

Velinsky, S.A., Anderson, G.L., Costello, G.A., 1984. Wire rope with complex cross sections. ASCE J. Eng. Mech. Div. 110, 380–391.